



Time-to-Functionality Fragilities for Performance Assessment of Buildings

Jace Furley, S.M.ASCE¹; John W. van de Lindt, F.ASCE²; Shiling Pei, M.ASCE³; Sarah Wichman, S.M.ASCE⁴; Hamed Hasani, A.M.ASCE⁵; Jeffrey W. Berman, A.M.ASCE⁶; Keri Ryan, A.M.ASCE⁷;

J. Daniel Dolan, F.ASCE⁸; Reid B. Zimmerman, M.ASCE⁹; and Eric McDonnell, M.ASCE¹⁰

Abstract: This paper presents a new stochastic methodology for evaluating and quantifying the downtime of a structure in terms of a family of fragilities that represent the probability of exceeding prescribed times to return to functionality. This methodology integrates several existing concepts, namely, Federal Emergency Management Agency P-58 and Resilience-based Earthquake Design Initiative (REDi), to build a family of system (building) level fragility curves corresponding to the time needed to achieve different recovery levels (reoccupancy, functional recovery, and full recovery). This approach enables one to propagate uncertainty throughout the procedure so that variations in the delay time and repair schedules are accounted for in the resulting fragilities. As an illustrative example of this approach, the methodology is applied to assess the downtime of a two-story mass timber building that was originally tested at the NHERI@UCSD outdoor shake table in 2017. One unique aspect of this analysis is that it incorporates a relatively new material, cross-laminated timber (CLT), in a resilient posttension rocking wall design application. Nonstructural components representing a typical office building were selected and incorporated into the procedure for the two-story CLT rocking wall building. Time-to-functionality fragility curves are then developed for the two-story building, and potential design and resilience-focused applications are discussed. **DOI: 10.1061/(ASCE)ST.1943-541X.0003195.** This work is made available under the terms of the Creative Commons Attribution 4.0 International license, https://creativecommons.org/licenses/by/4.0/.

Author keywords: Time-to-functionality; Fragility curves; Seismic design; Resilience; Reoccupancy; Functional recovery; Full recovery; Cross-laminated timber (CLT); Rocking wall.

Introduction

The ability to mitigate seismic risk with the application of a new design philosophy has garnered significant academic and professional

¹Graduate Student, Dept. of Civil and Environmental Engineering, Colorado State Univ., Fort Collins, CO 80523. Email: jace.furley@colostate.edu

²Harold H. Short Endowed Chair Professor, Dept. of Civil and Environmental Engineering, Colorado State Univ., Fort Collins, CO 80523 (corresponding author). Email: jwv@colostate.edu

³Associate Professor, Dept. of Civil and Environmental Engineering, Colorado School of Mines, Golden, CO 80401. Email: spei@mines.edu

⁴Graduate Student, Dept. of Civil and Environmental Engineering, Univ. of Washington, Seattle, WA 98195. Email: wichman@uw.edu

⁵Graduate Student, Dept. of Civil and Environmental Engineering, Univ. of Nevada Reno, Reno, NV 89557. ORCID: https://orcid.org/0000-0003-3018-1108. Email: hasani@nevada.unr.edu

⁶Thomas and Marilyn Nielsen Associate Professor, Dept. of Civil and Environmental Engineering, Univ. of Washington, Seattle, WA 98195. Email: jwberman@uw.edu

⁷Associate Professor, Dept. of Civil and Environmental Engineering, Univ. of Nevada Reno, Reno, NV 89557. Email: klryan@unr.edu

⁸Professor, Dept. of Civil and Environmental Engineering, Washington State Univ., Pullman, WA 99163. ORCID: https://orcid.org/0000-0002 -1331-6923. Email: jddolan@wsu.edu

⁹Technical Director/Associate, KPFF Consulting Engineers, 111 SW 5th Ave. #2600, Portland, OR 97204. Email: reid.zimmerman@kpff.com

¹⁰Principal, Holmes Structures, 555 SE Martin Luther King Jr. Blvd. Suite 602, Portland, OR 97214. Email: eric.mcdonnell@holmesstructures.com

Note. This manuscript was submitted on August 25, 2020; approved on July 27, 2021; published online on September 29, 2021. Discussion period open until February 28, 2022; separate discussions must be submitted for individual papers. This paper is part of the *Journal of Structural Engineering*, © ASCE, ISSN 0733-9445.

engineering attention, primarily in the form of performance-based seismic design over the last several decades. This trend has included studies focused on studying the effects of building performance on a community or urban area. In the United States, this increasing interest has manifested itself into initiatives such as the United States Resiliency Council (USRC) and the Seismic Resilience Initiative (SRI) (Sahabi et al. 2018). Specifically, in earthquake engineering, the growing interest in resilience is primarily due to a shift in design objectives. In the United States and across much of the world, seismic design has historically focused on life-safety objectives, with most current seismic design codes defining adequate performance of a structure simply as "life-safety" in a major event; meaning that occupants should be able to survive unharmed during a selected "design level" event. While life-safety remains the fundamental objective of any seismic design philosophy, additional impacts of a seismic event such as financial losses (both direct and indirect losses), societal disruptions, and adverse effects (e.g., population migration and community degradation) are now being considered more directly through modeling. This translates into a more comprehensive consideration of the resilience of a building system and the broader interconnected community network by including the ability to recover after an earthquake.

As indicated previously, a robust loss assessment methodology is critical to any second-generation performance-based seismic design (PBSD) approach or when incorporating resilience into a design. Consequently, in the past decade, research has focused on developing methods to predict the financial loss of individual buildings when subjected to a seismic event. Led by the Federal Emergency Management Agency (FEMA), these development efforts have culminated in a new approach to PBSD in FEMA P-58 (FEMA 2012a). FEMA P-58 details a five-step process to assess the seismic performance of a building, including assembling a building performance

model, defining earthquake hazards, analyzing building response, developing a collapse fragility, and calculating performance. The building performance in terms of tangible consequences is predicted from the structural response using fragility and consequence functions. Furthermore, the building's overall collapse fragility (probability of collapse as a function of ground motion intensity) is used specifically to help predict causalities in addition to other considerations (such as individual components). Consequence functions relate damage to the losses such as potential repair and replacement costs, repair time, casualties, unsafe placarding, and other impacts. Consequences are defined independently for each damage state (FEMA P-58). The performance assessment calculation tool (PACT) (FEMA 2012b) was developed to implement a Monte Carlo procedure based on Yang et al. (2009). Terzic et al. (2016) developed a repair model specifically designed to integrate easily with PACT utilizing the critical path method (CPM) to estimate the repair time. In addition, this model was designed to be an applicable repair model in a larger effort to determine the resiliency index of a building as defined in Cimellaro et al. (2010).

With a new, more robust, building level loss estimation methodology in place, it was now possible to complement larger-scale regional loss estimates such as the "ShakeOut Scenario" (a collaborative effort by government and academic entities to estimate the regional financial losses of a 7.8 magnitude earthquake on the southernmost 200 mi of the San Andreas Fault (Sahabi et al. 2018) with more comprehensive building level loss estimates. Prompted by the extensive losses seen in the devastating 2011 Christchurch, NZ earthquake, studies such as Terzic et al. (2012) and Mayes et al. (2013) implemented PACT to estimate financial losses of buildings designed to current prescriptive building codes. In the example presented in Mayes et al. (2013), the calculated losses could be in excess of 20% of replacement value, motivating the exploration of alternative design methods to reduce financial losses. Regional and individual building level studies including the discussed studies as well as many others help illuminate a distinct problem; there is a clear disconnect between what is considered adequate performance by prescriptive building codes (i.e., life-safety) and societal and stakeholder expectations (i.e., earthquake "proof") (Mayes et al. 2013). Terzic et al. (2014) performed a life-cycle cost analysis on five different designs of a hypothetical three-story steel office building located in Oakland, California. The designs included three fixed based designs: special concentrically braced frame (SCBF), special moment-resisting frame (SMRF), and viscously damped moment frame (VDMF) as well as two seismically isolated designs: baseisolated intermediate moment-resisting frame (BI-IMRF) and baseisolated ordinary concentrically braced frame (BI-OCBF). The authors found that in the assumed scenario, the BI-OCBF generated the best return on investment of all of the designs, with the lifecycle benefits outweighing the additional cost incurred during construction in comparison to the fixed base designs, and performed better than the more expensive BI-IMRF. Yamin et al. (2017) developed an economic loss estimation model that considers repair and commercial costs, incorporates both structural and nonstructural components, and assesses business interruption costs. This model was applied to a suite of archetypes, and vulnerability curves were constructed and compared to existing methods from HAZUS.

With the demand for more resilient building design well established, and robust tools such as PACT available, many government and academic entities began to develop evaluation systems for the resilience of a building. In 2013, the Resilience-based Earthquake Design Initiative (REDi) rating system was introduced. REDi is a comprehensive rating system considering the building resilience, organizational resilience, and ambient resilience (the resilience of structures surrounding the site) of a facility (Almufti and Willford 2013).

The system includes a three-level rating system (silver, gold, and platinum) as well as a detailed guide to the criteria at each level of the facility's operation, from utility operations after a seismic event to the design of the structural system, required to achieve a certain rating level (Almufti and Willford 2013). The USRC (2015) used REDi along with numerous other supporting materials to develop their own building rating system for earthquake hazards.

In this paper, a methodology is presented to develop timeto-functionality (TTF) fragilities, a major first step toward a full RBSD methodology. The approach presented adopts portions of FEMA P-58 and REDi methodology and combines it with other evaluation techniques to develop TTF fragility curves for use in a larger decision-making framework. As a proof of concept, the methodology was used to evaluate the performance of the two-story cross-laminated timber (CLT) rocking wall building with construction details available in Pei et al. (2019). CLT was identified as an excellent example for this methodology due to increasing interest in CLT as an alternative to traditional materials for midrise buildings, its demonstrated resilience capabilities when used as a posttensioned lateral system, and ongoing research efforts. A literature review on CLT is provided later in this paper with an illustrative example. It should be noted that in addition to the previously mentioned reasons, the two-story rocking wall structure was also selected because of the availability of rocking wall information from component level testing, design for a damage-free gravity system for the test specimen using pinned connections, and the increasing demand for better-performing wood buildings; the latter particularly for mass timber. Further, the authors' involvement in the testing of this specimen enabled better integration of the results with the new methodology in this study.

Methodology

Overview

The objective of the methodology presented in this paper is to develop fragility curves for the time it takes a building to become fully functional following a simulated earthquake (e.g., 60 days and 90 days). The TTF fragility curves are developed by evaluating the performance of structural and nonstructural components of the system subjected to a variety of ground motions at different intensities and integrating time and resource demands for repair and replacements. The evaluation of a full structure (particularly damage and corresponding repair process) induces significant uncertainty into the model, a multilayer direct Monte Carlo approach is used for evaluation.

Fig. 1 represents a flow chart of the methodology consisting of four major sections: (a) *Building Performance Model and Response Data (Steps 1–4)*, (b) *Loss Analysis (Steps 5–8)*, (c) *Repair Sequencing (Step 9)*, and (d) *TTF Fragility Curves (Steps 10 and 11)*.

The building performance model and Response Data Section consist of determining basic system characteristics such as structural and nonstructural components, quantities, and ground motion selection and scaling. It also incorporates the selection of the building performance model, which will determine the response of the structure to the scaled ground motions. The loss analysis determines the damage sustained by individual components using fragility and consequence functions from FEMA P-58. The Repair Sequencing Section determines the order in which components will be repaired and determines the TTF for the structure for a given realization. The REDi downtime assessment methodology is utilized in the Repair Sequencing Section to construct and evaluate a repair model for the structure and produce estimates of the system

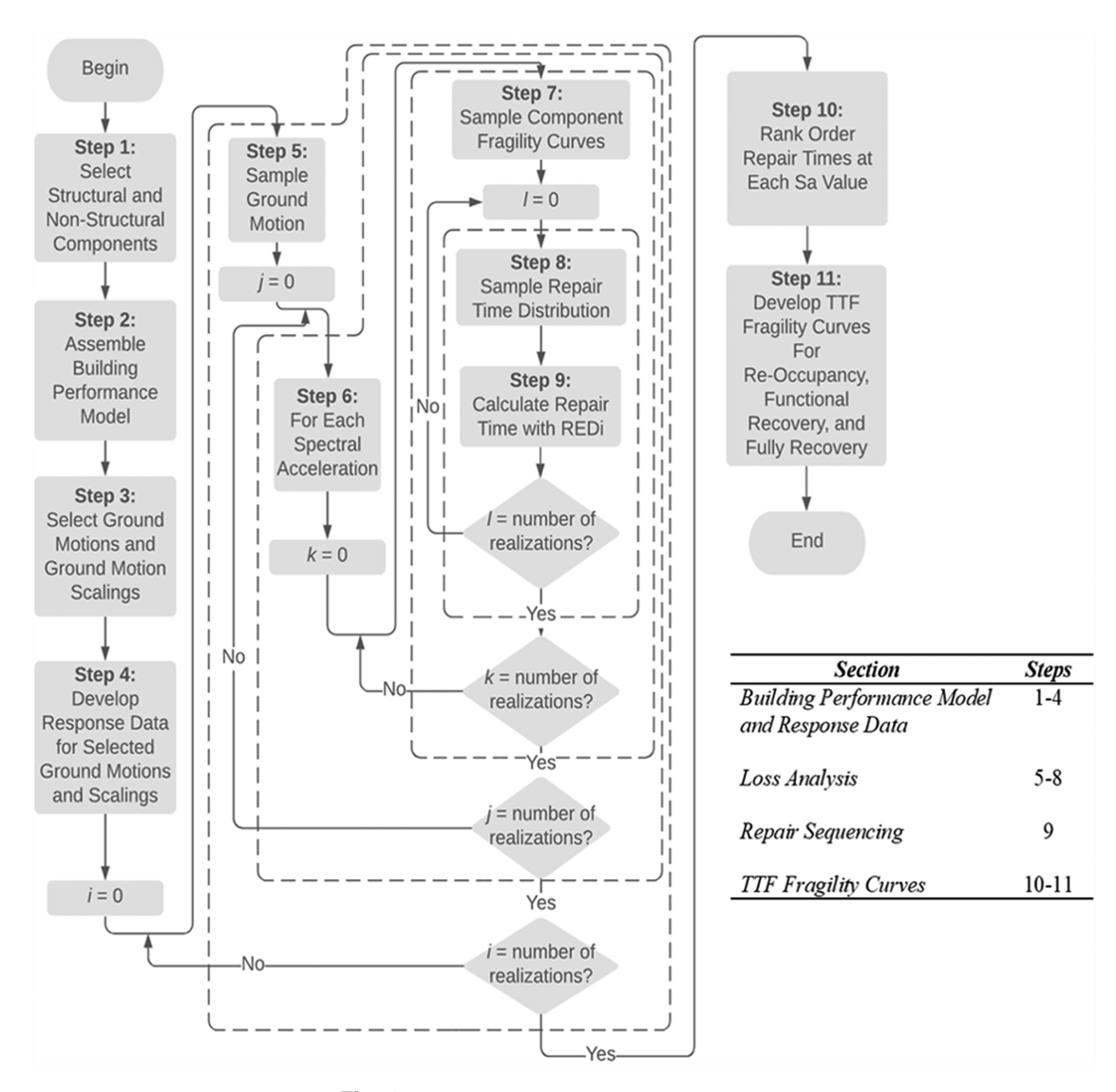


Fig. 1. Procedure for repair fragility generation.

level TTF. The TTF fragility curves represent the probability of a TTF being exceeded as a function of spectral acceleration (S_a) and they are developed by iterating the loss analysis and Repair Sequencing Sections over a number of realizations, each representing a different ground motion and scaling. The different levels of the Monte Carlo simulation are represented by the dotted lines and correspond to realizations i, j, k, and l in Fig. 1.

Building Performance Model and Ground Motion Requirements

As previously mentioned, the first section of the methodology (Fig. 1: Steps 1–4) includes identifying the structural and nonstructural characteristics of the system and the building performance model, which is typically a structural model to estimate engineering demand parameters (EDP), and selecting desired ground motions. Once the system, model, and motions have been selected, an analysis of the system excited by a suite of ground motions is performed with the response of the system determined by the selected building performance model. The remainder of the method operates on the EDP results; thus, the proposed procedure does not dictate the building dynamic modeling approach to be used, as long as it provides reasonably accurate EDP predictions. Similar to the model

selection, the ground motion selection and model analysis procedures are also quite flexible with either a typical incremental dynamic analysis (IDA) Vamvatsikos et al. (2002) or multistripe analysis Baker (2015) being viable. In general, the model analysis needs to produce vectors containing the EDPs for all spectral scalings at each story of the structure (specifically peak acceleration and interstory drift ratio), as associated with various scale factors for each of the selected ground motions. Additionally, the uncertainty introduced by the ground motion and model selection needs to be accounted for in the method. FEMA P695 (FEMA 2009) presents a methodology accounting for different sources of uncertainty (such as modeling, record-to-record, and test data) and is one suitable way to account for the various uncertainties.

Loss Analysis

The loss analysis of the system (Fig. 1: Steps 5–8) incorporates fragility and consequence functions for the nonstructural components that were developed for FEMA P-58. FEMA background documents provide documentation of the development of fragilities for individual components (e.g., Mosqueda 2016; Porter 2009a, b, c). In general, the fragilities have been developed through a combination

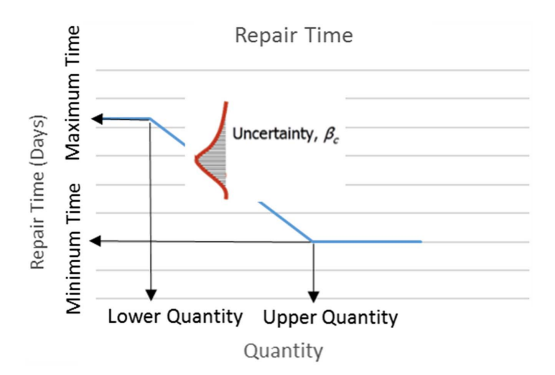


Fig. 2. Sample repair time function per FEMA P-58.

of laboratory testing, collection of historic earthquake data, structural analysis, and engineering judgment (FEMA 2012).

To support the methodology proposed here, repair time consequence functions were utilized. Specifically, each damage state includes a time-related consequence function indicating the number of labor hours associated with a specific repair. The actual time that a building will be unusable for reoccupancy following an earthquake is affected by many factors that make the reliable estimation of interruption time difficult (Mitrani-Reiser 2008). Thus, the consequence function method introduced in FEMA P-58 considers not only repair time, but also the time to procure needed resources, probability that a building will be posted with an unsafe placard, and influence of the overall occupancy interruption.

The fundamental parameter for developing repair time is the number of workers who can work in the building at the same time. The number of workers per square foot that may effectively occupy an area is limited, and FEMA P-58 provides an upper bound on this value. The repair time for each damage state is described using five parameters: lower quantity LQ (a quantity below which there is no reduction in efficiency), maximum repair time associated with the lower quantity RT_L , upper quantity UQ (the quantity above which there is no further gain in efficiency), minimum repair time associated with the upper quantity RT_U , and dispersion (uncertainty). Each point on the repair time versus quantity curve follows a lognormal or normal distribution (determined by experimental data), characterized by the lower and upper quantities (median values) and the dispersion (β). Fig. 2 represents a conceptual repair time consequence function featuring all the necessary parameters.

The repair time for all components and a single realization is represented by array $\mathbf{R}_{i,j,k,l}$ where i, j, k, l are the repair sample identification indices for ground motion, spectral acceleration, repair fragility curve, and time consequence function, respectively. To determine each repair time realization, a ground motion and scale factor are first randomly sampled (Fig. 1: Steps 5 and 6), with the distribution of ground motions represented by $g(\boldsymbol{\theta}_{i,j}|\boldsymbol{M})$ where $\theta_{i,j}$ is the demand parameter result array (interstory drift ratios or acceleration) determined by the building performance model for given motions M. The component level fragility curves are then sampled to determine damage states for each component (Fig. 1: Step 7). These fragilities are randomly sampled from $P_{i,j,k} \sim U(0,1)$, where $P_{i,i,k}$ is the probability of occurrence array given probability sample k, spectral acceleration j, and ground motion sample i. Then, using $P_{i,j,k}$ and $\theta_{i,j}$, damage states for each component are determined using their associated fragility curves. Damage states are represented by $D(DS_{i,j,k}|\boldsymbol{\theta}_{i,j}, \boldsymbol{P}_{i,j,k}, \boldsymbol{\pi})$ where $DS_{i,j,k}$ is the damage state array; $\theta_{i,j}$ is the demand (peak interstory drift ratio or floor acceleration); $P_{i,i,k}$ is the probability of occurrence; and π are the fragility curves. The final step in the *loss analysis* is to sample the repair time probability density functions (pdf) for the components given the determined damage state (Fig. 1: Step 8). The pdf of a component is either lognormal or normal depending on the experimental data fit, and the mean of the distribution is determined using the quantity of the component and the sample repair time consequence function. The component pdf is then sampled to determine the time realization array $R_{i,j,k,l}$. This can be represented as $RD(R_{i,j,k,l}|DS_{i,j,k},II)$ where $R_{i,j,k,l}$ is the repair time realization array given damage state $DS_{i,j,k}$ and component pdfs II. This deviates from FEMA P-58 in that it considers all repair time samples, while FEMA P-58 methodology uses the 90th percentile of the repair time samples in its calculations.

Repair Sequencing Using REDi Methodology

Once the repair times for all of the individual components are estimated for a realization (Fig. 1: Steps 1-8), the system level TTF is calculated (Fig. 1: Step 9). There are a variety of considerations to accomplish this objective. First, the component importance needs to be considered. For example, using typical best practice and engineering judgment, certain elements such as structural components are the primary concern and are typically repaired first, with other nonstructural components such as partition walls and suspended ceiling tiles being of secondary or tertiary concern. The REDi downtime assessment methodology provides a relatively comprehensive database of repair priorities corresponding to the fragility data in PACT. The data were compiled using various methods including testing results and expert opinions of engineering and architectural professionals (Almufti and Willford 2013). This methodology categorizes the components of the structure into three distinct classes corresponding to a system recovery or operation, as can be seen in Table 1. It should be noted the worker allocation and repair sequencing algorithm is based on the REDi defined repair classes, repair priority, and repair sequencing. So the algorithm considers priority of repair, sequence of repair, material lead time, number of allocated workers, and maximum number of workers per sq. meter. Thus, a limitation of this method is that the likelihood of repairing similar components on different floors is not directly considered.

The system recovery levels, namely, reoccupancy, functional recovery, and full recovery, are each defined by the amount of time to repair the components in their repair class (3, 2, and 1 respectively) to regain a certain level of functionality to the structure. Reoccupancy is defined as the minimum amount of time required for the structure to safely be used as shelter. For functional recovery, reoccupancy demands must be met in addition to the time required for the structure to regain its primary function. Finally, to achieve full

Table 1. REDi repair classes and system recovery levels

| Repair class | Repair description |
|-----------------|--|
| 3 | Heavily damaged nonstructural or structural components that pose a life-safety risk and must be repaired for reoccupancy |
| 2 | Damaged nonstructural components that inhibit the functionality of the structure, but do not pose a life-safety risk; required for functional recovery |
| 1 | Minimal or minor cosmetic damage to structural or nonstructural components that inhibit the return of the structure to its prehazard state: required for full recovery |

Source: Data from Almufti and Willford (2013).

Table 2. REDi impeding factors distribution

| Impeding factor | Building | Mitigation measure | Other conditions | β | θ |
|--------------------------|------------------------|--------------------------|-------------------------|----------|----------|
| Inspection | All facilities | BORP equivalent | _ | 1 day | 0.54 |
| | Essential facility | | _ | 2 days | 0.54 |
| | Non-essential facility | _ | _ | 5 days | 0.54 |
| Engineering mobilization | All facilities | Engineer on contract | Max structural RC = 1 | 2 weeks | 0.32 |
| and review/redesign | | | Max structural $RC = 3$ | 4 weeks | 0.54 |
| | | | Complete redesign | 42 weeks | 0.45 |
| | | _ | Max structural $RC = 1$ | 6 weeks | 0.40 |
| | | | Max structural $RC = 3$ | 12 weeks | 0.40 |
| | | | Complete redesign | 50 weeks | 0.32 |
| Financing | All facilities | Pre-arranged Credit line | _ | 1 week | 0.54 |
| | | _ | Insurance | 6 weeks | 1.11 |
| | | _ | Private loans | 15 weeks | 0.68 |
| | | _ | SBA-backed loans | 48 weeks | 0.57 |
| Contractor mobilization | Essential facility | GC on contract | Max RC = 1 | 3 weeks | 0.66 |
| | <20 stories | | Max RC = 3 | 7 weeks | 0.35 |
| | | _ | Max RC = 1 | 7 weeks | 0.60 |
| | | | Max RC = 3 | 19 weeks | 0.38 |
| | Non-essential facility | GC on contract | Max RC = 1 | 3 weeks | 0.66 |
| | <20 stories | | Max RC = 3 | 7 weeks | 0.35 |
| | | _ | Max RC = 1 | 11 weeks | 0.43 |
| | | | Max RC = 3 | 23 weeks | 0.41 |
| | ≥20 stories | GC on contract | Max RC = 1 | 3 weeks | 0.66 |
| | | | Max RC = 3 | 7 weeks | 0.35 |
| | | _ | Max RC = 1 | 28 weeks | 0.30 |
| | | | Max RC = 3 | 40 weeks | 0.31 |
| Permitting | All facilities | _ | Max structural RC = 1 | 1 week | 0.86 |
| | | _ | Max structural $RC = 3$ | 8 weeks | 0.32 |

Source: Data from Almufti and Willford (2013).

recovery, the building must be repaired to its pr-earthquake condition (Almufti and Willford 2013).

Once the priority of component repair is determined, a repair schedule is developed. The repair schedule is dependent on factors such as worker availability, component lead times, and intercomponent dependencies. This includes parallelization, allocation, and the number of workers per floor using a grouping system for components where similar components are assigned to a single group and workers are allocated to each group as an entity. Every group or repair sequence can be in parallel except for the structural component group, and it is assumed that structural components are completely repaired prior to any nonstructural repair (Almufti and Willford 2013). In addition, impeding factors such as inspection, engineering mobilization, financing, contractor mobilization, and permitting are estimated using normal distributions. The estimated distributions vary by the facility type, story number, mitigation measure, maximum structural/nonstructural damage, and financing source as seen in Table 2. β and θ represent the mean and dispersion for a normal distribution.

The resulting repair schedule is then constructed for a time corresponding to each recovery level (reoccupancy, functional recovery, full recovery). A universal total TTF for the structure for one realization can be represented by

$$[\mathbf{RO}_{i,j,k,l}, \mathbf{FR}_{i,j,k,l}, \mathbf{FuR}_{i,j,k,l}] = r(\mathbf{R}_{i,j,k,l}) \tag{1}$$

where $\mathbf{R}_{i,j,k,l}$ = repair time realization array from the *loss analysis* procedure (Fig. 1: Steps 5–8); $r(\mathbf{R}_{i,j,k,l})$ = repair sequencing function (Fig. 1: Step 9); and $\mathbf{RO}_{i,j,k,l}$, $\mathbf{FR}_{i,j,k,l}$, and $\mathbf{FuR}_{i,j,k,l}$ = TTF values corresponding to realization i, j, k, l (corresponding to ground motion sample i, spectral acceleration j, probability sample k, and repair time sample l, respectively) for reoccupancy, functional

recovery, and full recovery, respectively. In addition, it should be noted that the form of the repair sequencing function is left arbitrary to reflect the form flexibility of the function. In the later example, an algorithm is used as the repair sequencing function, but the form of the repair sequencing function is not determined by the method.

Time-to-Functionality Fragility Curves

With the process and equations developed for determining reoccupancy, functional recovery, and full recovery for an iteration, equations are developed to represent the multilayered direct Monte Carlo, as follows:

$$\hat{H}_K = \frac{1}{K} \sum_{i=1}^K g(\boldsymbol{\xi}_i) \tag{2}$$

where \hat{H}_K = estimator; K = number of samples; and $g(\xi_i)$ = model evaluated at a sample point. The multilayer Direct Monte Carlo can therefore be represented by

$$\hat{\boldsymbol{H}}_{K_{i,j}} = \frac{1}{K} \sum_{k=k}^{K} \frac{1}{L} \sum_{l=1}^{L} r(\boldsymbol{R}_{i,j,k,l})$$
 (3)

where $\hat{\boldsymbol{H}}_{K_{i,j}}$ = estimator array for reoccupancy, functional recovery, and full recovery for motion i and spectral acceleration j. Equation $r(\boldsymbol{R}_{i,j,k,l})$ is the repair sequencing function with repair time realization array $\boldsymbol{R}_{i,j,k,l}$ given samples ξ_k , ξ_l and demand parameter array $\boldsymbol{\theta}_{i:k}$.

Utilizing estimator $\hat{\boldsymbol{H}}_{K_{i,j}}$, repair fragility scatter plots can be developed for reoccupancy, functional recovery, and full recovery, respectively (Fig. 1: Step 10). This is accomplished by rank ordering the total times at each spectral acceleration (Sa) as

$$P_{E_{i,j}} = \frac{m_{i,}}{n_j} \tag{4}$$

where m = rank order of estimator $\hat{H}_{K_{i,j}}$ (time to functionality) for ground motion record i at Sa j; n = total number of realizations at Sa j; and $P_{E_{i,j}}$ = probability of exceedance for the TTF for motion i at Sa j. The interval at which repair fragility scatter plots can be developed is limited by the resolution of repair data provided by PACT, i.e., person-days. Once plots have been developed, individual TTF data are fit using a lognormal cumulative distribution function (CDF) of the form

$$F_X(x) = \Phi\left(\frac{\ln x - \mu}{\beta}\right) \tag{5}$$

where μ = mean; and β = dispersion of the logarithmic samples for each of the TTF fragility scatter plots (Fig. 1: Step 11). It should be noted that in this study lognormal fragility fits were assumed for convenience. The resulting family of fragility curves presents information on the probability of exceedance for a variety of TTF values for the structure developed using multiple demand parameters, representing a concise summary of the structure's predicted performance. This information can then be used to set performance objectives for the structure and can fit into a larger decision framework on the selection of structural and nonstructural components to reduce TTF. Further, the effect of cost to improve certain classes of building type could be weighed against the change in community-level recovery or resilience (Ellingwood et al. 2016) in order to modify the current building code.

Illustrative Example: Two-Story CLT Building with Rocking Walls

Over the past 15 years, significant strides have been made in demonstrating the effectiveness of CLT as both a traditional seismic force-resisting system (SFRS) and a resilient alternative. Beginning in the early 2000s, researchers investigated the applicability of CLT in moderate to high seismic zones. Early studies (Dujic et al. 2004, 2006) focused primarily on platform construction and identified connections as the primary source of ductility for CLT lateral forceresisting systems, while connection failures and local wood failures were the primary failure modes. The SOFIE project incorporated earlier work into a full-scale 7-story CLT platform building shake table test (Ceccotti et al. 2013). The testing demonstrated the suitability of mass timber with CLT for midrise buildings while simultaneously identifying deficiencies and future research needs. However, during this shake table test program and other previous tests, CLT platform buildings demonstrated a vulnerability from large accelerations and overturning moments. In North America, significant recent research efforts (Popovski et al. 2010, 2012, 2016; Pei et al. 2013, 2016; Amini et al. 2014) have focused on CLT buildings, including experimental testing and development of seismic performance factors.

Resilient mass timber seismic research began in New Zealand in the mid2000s with the adaptation of a rocking wall concept originally used in concrete walls, applying the concept to laminated veneer lumber (LVL) and investigating different moment connections and posttensioning configurations (Palermo et al. 2006). This early research laid the groundwork for the further development of a posttensioned lateral force-resisting rocking wall system capable of utilizing a variety of mass timber products (Buchanan et al. 2008). Posttensioned rocking walls made from LVL were eventually incorporated into a number of commercial projects including the 3-story Arts & Media Building in Nelson, NZ (Holden et al. 2012).

The success of the system inspired component tests implementing CLT instead of LVL, with the specific intention of improving the ductility of contemporary lateral force-resisting systems in CLT buildings (Ganey et al. 2017). Akbas et al. (2017) derived model parameters from the experimental test data of Ganey et al. (2017). These results were then used to design a full-scale shake table test of a two-story CLT building with posttensioned rocking walls. The experiment demonstrated the resilience capabilities of the system; the building recentered without unintended structural damage after each of a series of 14 earthquakes and sustained interstory drift ratios far beyond design level, i.e., up to 5% (Pei et al. 2019). CLT resilient design has been making strides in recent years, and a resilient CLT structural system suitable for midrise buildings was demonstrated to be effective in small- and large-scale testing. However, the current resilient design for CLT only considers the structural system itself, thereby underscoring the need to incorporate other nonstructural systems into the design.

Building Overview

The TTF fragility curve methodology described is applied herein to a two-story mass timber building with posttensioned CLT rocking walls as the SFRS. The previously mentioned two-story CLT building with posttensioned CLT rocking walls was tested at the University of California, San Diego's shake table, Natural Hazards Equipment Research Infrastructure (NHERI)@UCSD, in 2017. The building floor diaphragms were 6.10 m \times 17.68 m (20 ft \times 58 ft) in plan and the story heights were 3.66 m (12 ft) and 3.05 m (10 ft), respectively. The main force-resisting structural system consisted of two 7.32 m (24 ft) tall CLT posttensioned rocking walls, each comprised two CLT rocking wall panels sets of posttensioned CLT rocking walls coupled together using five U-shaped flexural steel plates (UFP), as well as CLT diaphragms. The gravity framing consisted of glulam columns and beams. The approximate seismic mass on the floor and roof level was 4.19×10^3 kg (92.4 kips) and 4.31×10^3 kg (95.1 kips). The test structure including the lateral and gravity systems can be seen in Fig. 3. As mentioned, each CLT rocking wall was made of two coupled CLT wall panels. Each wall panel was 1.52 m (5 ft) wide and made of 5-ply CLT with a thickness of 175 mm (67/8 in.). Each panel was externally posttensioned with four high-strength, fully-threaded, 19 mm (3/4 in.) diameter rods with yield strengths of 634 MPa (92 ksi). Each bar was initially posttensioned to a force of 53.4 kN (12 kips). There were two bars on either



Fig. 3. Two-story CLT building with posttensioned rocking walls. (Image by authors.)

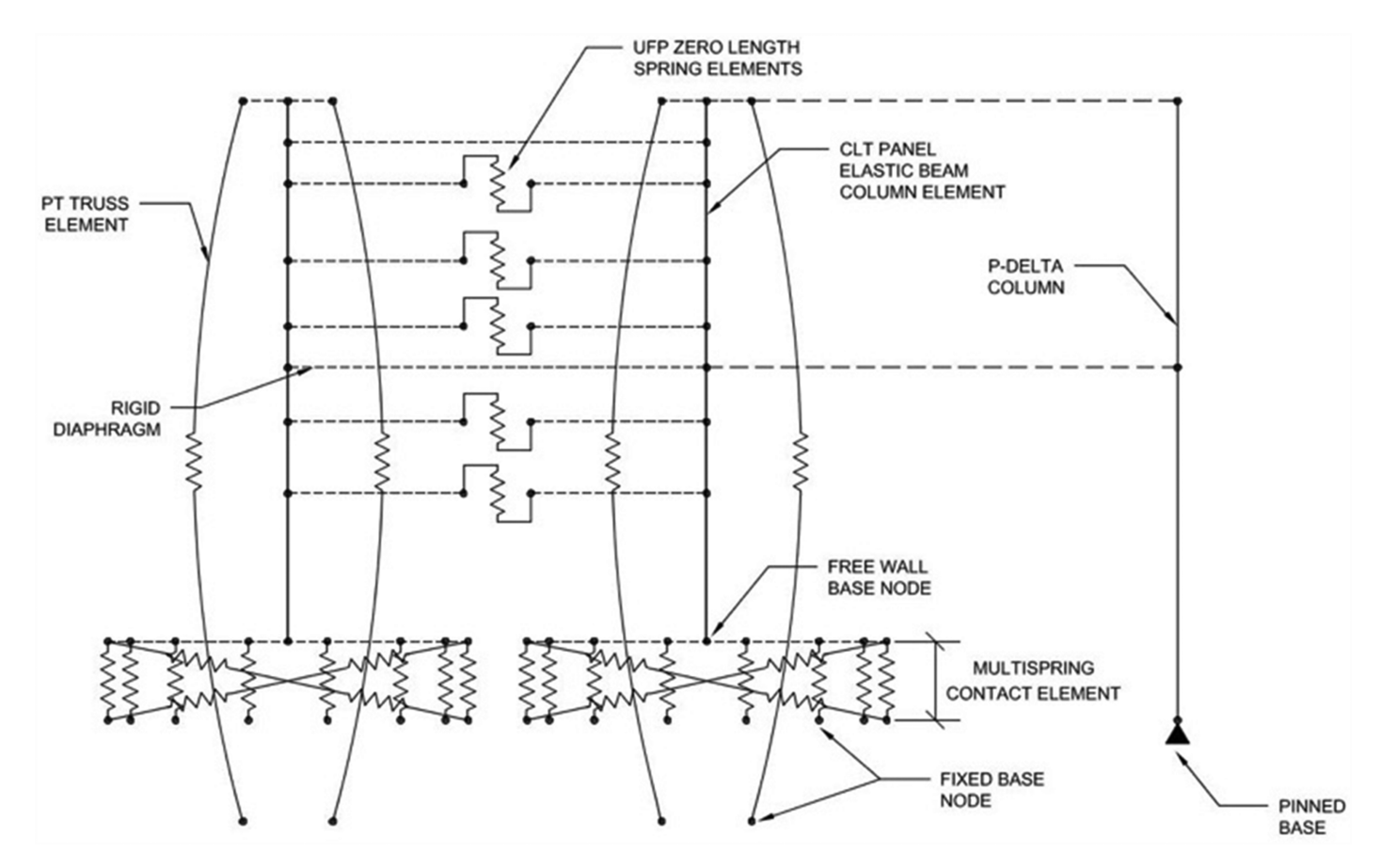


Fig. 4. OpenSees numerical model schematic for the coupled CLT rocking walls used in analysis.

face of the wall panel and spaced at 254 mm (10 in.) from the centerline of the panel. The five UFPs coupling each wall had a diameter of 92 mm (35/8 in.), a width of 114.3 mm (4½ in.), and a thickness of 9.5 mm (3/8 in.) (Pei et al. 2019).

Building Performance Model and IDA

Numerical modeling of the posttensioned CLT rocking walls was performed using OpenSees (Mazzoni et al. 2009). The *building performance model* as seen in Fig. 4 consisted of six main components: (1) elastic Timoshenko beam-column wall elements, (2) multispring contact elements, (3) posttensioned (PT) bar truss elements, (4) UFP spring elements, (5) rigid diaphragm elements, and (6) a P-Delta column. This model utilized modeling concepts originally developed by Ganey (2015). Because the test building was symmetric and experienced very little accidental torsion, a two-dimensional model was used where only one of the two coupled CLT rocking walls was modeled, representative of half the building.

The elastic portion of the walls was modeled using a series of elastic Timoshenko beam-column elements. An elastic modulus of 8536 MPa (1238 ksi) was used based on material compression tests completed by Oregon State University (Barbosa et al. 2018). The first element spanned from the free wall base node to the location of the first UFP, the subsequent elements spanned between the UFP locations and the diaphragm locations on the panels, and the last element spanned from the roof diaphragm connection to the top of the wall. The nonlinear rocking behavior of the panels and the compressive deformation of the CLT were modeled using a multispring contact element at the base of each panel initially developed by Spieth et al. (2004). The multispring contact element consisted of 40 parallel zero-length springs spaced along the length of the

base of the panel in accordance with a Gauss–Lobatto integration. The top of each spring was linked by a rigid element to the free wall base node, while the bottom of each spring was fixed. Each spring was only allowed to deform axially and was defined with an elastic-perfectly plastic, compression-only material model to model the CLT compression behavior and the gap opening at the base of the panel. The compression contact stiffness, K_s , for each multispring element was calculated as

$$K_s = \frac{AE}{L_p} \tag{6}$$

where A= weighted cross sectional area of the CLT panel; E= elastic modulus of the CLT; and $L_p=$ assumed plastic hinge length. In this model, a plastic hinge length of $2b_w$ was assumed in accordance with Akbas et al. (2017), where b_w is the thickness of the wall panel. A CLT yield strain of 0.0029 was assumed for the onset of yielding in these springs, also determined in accordance with the tests completed in Barbosa et al. (2018). Finally, a diagonal shear spring, connecting the corners of each multispring contact element, was used to transfer shear at the base of the panels.

The posttensioned bars were modeled using tension-only corotational truss elements. In tension, a bilinear hysteretic material model was used. These elements were fixed at the base and connected to a rigid element spanning from the location of the PT bar to the top center of the panel. The stiffness of the PT elements was determined using Hooke's law for a truss element. An initial strain was also applied to the bars to model the initial posttensioning. It should be noted that because bars were located on either face of the wall panels, and each PT element shown in Fig. 4 is representative of two bars in the structure.

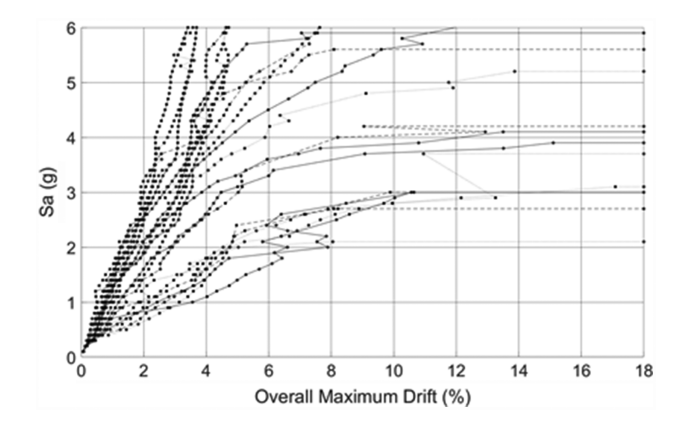


Fig. 5. FEMA P695 suite IDA curves for two-story CLT test structure.

Each UFP was modeled with a zero-length spring incorporating a uniaxial Giuffrè-Menegotto-Pinto steel material model with isotropic strain hardening. A rigid element connected each elastic beam-column element at the center of the wall panel to the zero-length UFP spring located between the two wall panels. The stiffness and peak UFP forces used in the model were calculated according to Baird et al. (2014). At the diaphragm levels, rigid truss elements were used to link the two wall panels. Gravity loads and associated inertial forces were represented using the leaning column approach, whereby an additional pinned-pinned P-Delta column representing the tributary gravity framing was connected to the wall system.

Next, a suite of 22 ground motions from FEMA P695 (FEMA 2009) was selected, and IDA was performed (Fig. 5). In IDA, each motion is incrementally scaled to different Sa values until the IDA curve flattened and collapse was identified. The flatting of the curve is significant because the IDA curve is plotted interstory drift ratios versus Sa in this case and so would indicate very large drift increases with minimal Sa increases, i.e., collapse. This produced vectors of peak interstory drift ratios and peak floor acceleration for each story of the structure that are functions of both spectral acceleration and ground motion that are used in the loss and repair analysis of the building.

Loss Analysis

Structural Fragility Selection

While the FEMA P-58 database contains a large collection of fragility information for a variety of structural components such as reinforced concrete and steel, there is a lack of information on mass timber products. In this study, results from existing experimental and analytical studies on an isolated posttensioned CLT rocking wall (Akbas et al. 2017; Ganey et al. 2017) were used to approximate the various damage states (Table 3) of the rocking wall system. Note that it would also be possible to characterize the fragility of the rocking wall system by its constituent parts (e.g., the wall itself, UFPs, and PT bars) separately and will likely be done in future analyses.

Several of the damage states would be difficult to detect with typical inspection techniques, and would be interpreted as no damage; thus, they are not included in the repair activity (i.e., downtime). As a result, the ELL and YCLT damage states were not considered in this example due to their detection difficulty, and the remaining damage states were considered in the analysis. Structural monitoring could assist in tracking damage levels for the PT rocking wall with

Table 3. CLT rocking wall damage states

| Damage state | ELL | YUFP | YCLT | SCLT | CCLT | LLP |
|----------------------------|-----|------|------|------|------|-----|
| Interstory drift limit (%) | 0.4 | 1.6 | 1.7 | 4.6 | 7.3 | 4.2 |

Sources: Data from Akbas et al. (2017); Ganey et al. (2017). Note: ELL = effective linear limit; YUFP = yielding of UFPs; YCLT = yielding of CLT; SCLT = splitting of the CLT (exceedance of the splitting strain at compression edge of the wall); CCLT = crushing of CLT (exceedance of the compression strain at compression edge of wall); and LLP = yielding of PT bars.

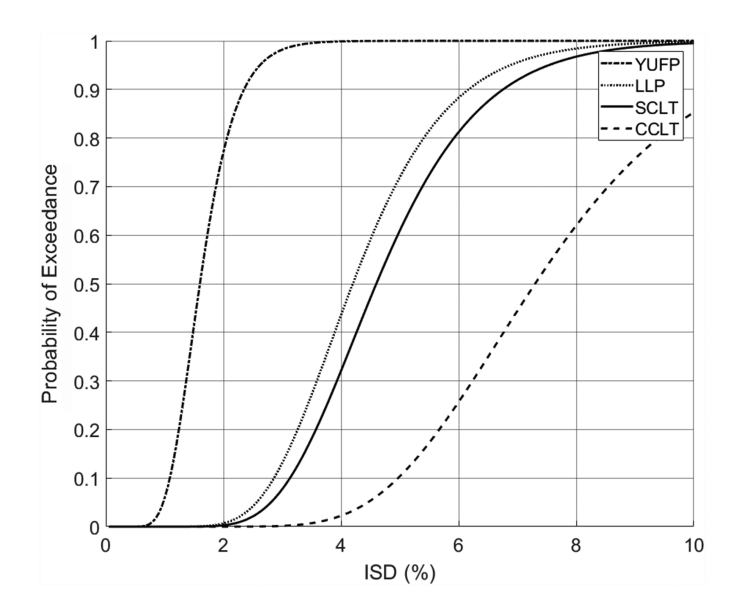


Fig. 6. Illustrative CLT posttensioned rocking wall fragility curves.

either strain gages or displacement measurements that utilize structural analysis to back out likely points of damage state limits. To develop the fragility curves from these deterministic drift damage state limits, several assumptions were made. Primarily, the drift limit was assumed to represent the mean value in a lognormal fragility curve, and a dispersion value of $\beta=0.3$ was selected to represent the expected variation in the drift limit states. These assumptions resulted in the rocking wall fragility curves shown in Fig. 6.

Although modeling uncertainty and ground motion uncertainty are often considered in the development of damage fragilities, i.e., particularly collapse fragilities [see FEMA P695 (FEMA 2009)], adoption of existing component fragilities combined with several component fragilities from experimental results was felt to be adequate for the illustrative example without adding additional dispersion to the fragility. This is mainly because the focus on the functionality fragilities adds another layer of dispersion through the application of the multilayer MCS approach. It is likely that mean values for the time to functionality are fairly well preserved, but there may be errors introduced in the tails, e.g., 90th or 95th probability of nonexceedance.

In many buildings, the gravity connections should also be included as damageable components. However, in the present case, the connections were designed as pinned and remained undamaged during a large number of high-intensity seismic tests (Pei et al. 2019); thus, it was not possible to include them in the model.

There is believed to be no research on repair time consequence functions for a CLT rocking wall at the time of writing. Thus, repair time consequence functions were determined using engineering judgment and CLT experience of the authors, see Table 4.

Table 4. Summary of repair times of CLT rocking wall in a two-story building example

| | | | | Repair time (person-days) | | | |
|--|-----|-------------------------------------|---------|---------------------------|----------|----|-------------------|
| Category | EDP | Damage state description | Q | LQ | RT_{L} | UQ | RT_{U} |
| CLT rocking wall—lateral force-resisting | SDR | Yielding of UFPs | SM 22.3 | 2 | 2 | 10 | 1 |
| system including PT bars, two CLT walls, | | Yielding of PT bars | | | 2 | | 1 |
| and UFP connectors | | Crushing of CLT | | | 23 | | 23 |
| | | Splitting of the composite material | | | 23 | | 23 |

Note: EDP = engineering demand parameter; SDR = story drift ratio; Q = quantity; LQ = lower quantity; UQ = upper quantity; and SM = square meter.

In addition, a normal distribution was assumed to represent the variation in repair times (similar to PACT) with the mean being the interpolated repair time based on the quantity and an assumed dispersion of $\beta=0.3$ for all damage states. While the lack of information on CLT rocking walls and diaphragms is not ideal, it should be noted that similar to the gravity frame and diaphragm, the rocking wall would remain mostly undamaged at practical intensities. Thus, minor variations in the rocking wall repair time consequence functions should not translate into a significant change in global time to functionality.

Nonstructural Fragility Selection

Note that the CLT structure was tested in 2017 without nonstructural systems, and the nonstructural component data was added for this illustrative example. Fragility and consequence functions for the most damageable nonstructural components were incorporated, based on a review of previous loss estimation studies (Zeng et al. 2016; Cutfield et al. 2016). Selected components include partition walls, glazing, suspended ceilings, cooling towers, chillers, compressors, HVAC systems, and sprinkler-piping systems. For each component for which multiple fragility functions have been developed to represent detailing variations, the most modern and resilient detailing was selected to meet the resilient design objectives of a timber building with a posttensioned rocking wall. For example, for partition walls, slip-track detailing was selected over fully fixed connections for its ability to absorb drift by sliding of the top track (Hasani et al. 2018). Table 5 summarizes the components utilized in this study based on FEMA P-58 classifications, EDP upon which damage is assessed, potential damage states associated with the components, basic quantity unit Q, and lower and upper quantities and repair times.

Some limitations should be noted. First, FEMA P-58 data are not complete for all possible components attached to a building. For example, fragilities for equipment such as cooling towers, chillers, and compressors are categorized as equipment fragilities, anchorage fragilities, and combined fragilities. However, anchorage fragilities for anchoring the equipment to the building are not given. The background documents related to this equipment (Porter 2009a, b, c) provide only combined fragilities for the anchored components, which are no longer utilized. This is due to the building-specific nature of anchorage design, making it difficult to generalize. The consequence functions are also reliant on the quantity of materials to determine the repair distribution, and since only structural components were included in the full-scale testing, the nonstructural component quantities were estimated. The building was considered as a two-story office building and typical quantities of nonstructural components were estimated for the square footage of the structure. For this purpose, the ground and second floor were classified as office occupancy, and all HVAC equipment was located on the roof. It should be noted that the selected HVAC elements are larger than required for the square footage due to the test building being smaller than a typical office building.

Repair Sequencing

The repair sequencing for the two-story structure consisted of interpreting the components (CLT SFRS and nonstructural) for use in the REDi downtime assessment methodology (Almufti and Willford 2013). Repair classes were selected for each of the components. As previously mentioned, repair classes determine the priority of repair for the component. For the majority of the components, repair classes have been predefined as part of the development of the methodology. The CLT rocking wall, however, has not been considered in REDi, so repair classes needed to be defined. After minor damage, i.e., damage state 1, the CLT rocking wall system is believed to have enough remaining lateral capacity to be considered safe for occupation. However, because of the potential yielding of the UFPs, it was conservatively assumed that the structure would be tagged with a yellow placard (restricted use) by inspection after a minor event in accordance with FEMA P-58. This is interpreted as repair class 3 as defined in Table 1 for all damage states considered. It would also be possible to store extra UFPs on site to reduce lead time for fabrication. Descriptions and selected repair class priority for all considered components are summarized in Table 6. It should be noted that the average damage state for a component across a floor is used for the repair class determination. This is primarily done as a simplification as well as an indicator for the damage of the component across an entire floor.

Synthesis of Time-to-Functionality Fragility Curves

TTF fragility curves were developed using the previously described rank-ordering method with a density of one day; 5,000 ground motion realizations were considered, resulting in the equivalent amount of individual time samples for each of the recovery levels (reoccupancy, functional recovery, and full recovery). The data for each day were assumed to correspond to a lognormal distribution of the previously described form, and with this assumption, fragility curves were fit to the data. Fig. 7 shows the reoccupancy TTF scatter plot as well as fitted reoccupancy fragility curves, while Fig. 8 presents only the fitted reoccupancy fragility curves and the corresponding fit data for 86 days, 95 days, 120 days, 140 days, and 182 days. The TTFs were chosen to represent the behavior of the TTF family of curves, apart from the 182 day TTF. This was chosen to represent approximately 6 months and a 3-star resilience rating as defined by the USRC. The other four ratings (5 days, 4 weeks, 1 year, and more than 1 year) were not included due to the TTF behavior of the structure. The impeding factors previously discussed in detail prevent 5 days and 4 weeks from being feasible for any damage beyond no damage. 1 year and greater than 1 year are near or exceed the maximum TTF determined from the simulation and therefore are not realistic to consider for this structure.

Observing the scatter plot in Fig. 7, two phenomena become apparent. First, there is a relatively low density of points for lesser TTF values (such as 86 days). This can be explained by the stochastic nature of the simulation. Data in this region represent moderate to

Table 5. Summary of repair time of nonstructural components in a two-story building example

| | | | | Re | pair time | (person | ı-days) |
|--|------|---|-----------|----|----------------------------|---------|-------------------|
| Category | EDP | Damage state description | Q | LQ | RT_{L} | UQ | RT_{U} |
| C1011.001c–partition wall–gypsum with metal studs–fixed below, slip track above | SDR | Minor damage that can be repaired without replacement of wallboard. | SM 120.8 | 1 | 1.36 | 10 | 0.366 |
| | | Severe damage such that replacement of wallboards is necessary. | | | 2.85 | | 0.863 |
| | | Damage to wallboard and framing (replacement of wall is necessary). | | | 5.46 | | 1.64 |
| B2022.011—glazing-midrise stick-built curtain | SDR | Gasket seal failure. | SM 2.8 | 20 | 0.905 | 100 | 0.482 |
| wall, configuration: asymmetric insulating glass | | Glass cracking. | | | 1.3 | | 0.696 |
| units, laminated, annealed, | | Glass falls out. | | | 1.04 | | 0.74 |
| C3032.003a—ceiling–suspended ceiling, SDC D, E | PFA | 5% of ceiling grid and tiles damaged. | SM 23.2 | 1 | 0.697 | 10 | 0.211 |
| (Ip = 1.0), area (A): A <250, Vert and Lat support | | 30% of ceiling grid and tiles damaged. | | | 5.41 | | 1.62 |
| Dana4 0001 11 | DE. | 50% of ceiling grid and tiles damaged. | | | 11.2 | _ | 3.34 |
| D3031.023b–cooling tower–capacity: <100 t–equipment that is either hard anchored or is vibration isolated with seismic | PFA | Damage to equipment and attached piping but the anchorage is OK. | EA 1 | 1 | 8.36 | 5 | 2.79 |
| snubbers/restraints-equipment fragility only | | | | | | | |
| D3031.013b-chiller-capacity: <100 t-equipment | PFA | Damaged, inoperative but anchorage is OK. | EA 1 | 1 | 14.3 | 5 | 4.76 |
| that is either hard anchored or is vibration | | | | | | | |
| isolated with seismic snubbers/restraints-equipment | | | | | | | |
| fragility only | P.F. | | | | 0.0=4 | _ | 0 =04 |
| D3032.013b compressor–capacity: small | PFA | Equipment does not function but the | EA 1 | 1 | 0.971 | 5 | 0.794 |
| non-medical air supply-equipment that is either | | anchorage is OK. Motor is damaged. | | | 0.605 | | 0.150 |
| hard anchored or is vibration isolated with seismic | | Equipment does not function but the | | | 0.635 | | 0.159 |
| snubbers/restraints-equipment fragility only | | anchorage is OK. Equipment damaged beyond repair. | F. 40 | | 0.06 | _ | |
| D3041.002c HVAC fan in line fan, fan | PFA | Bellows fail at fans. | EA 10 | 1 | 9.06 | 5 | 7.41 |
| independently supported but not on vibration | | | | | | | |
| isolators, SDC D, E, F | DE. | | | | 0.041 | - | 0.600 |
| D3041.011c HVAC galvanized sheet metal ducting | PFA | Individual supports fail and duct sags–1 | LM 92.9 | 1 | 0.841 | 5 | 0.688 |
| less than 6 sq. ft in cross sectional area, SDC D, E, or F | | failed support per 1,000 ft of ducting. | | | 2.00 | | 1 40 |
| | | Several adjacent supports fail and sections | | | 2.99 | | 1.49 |
| | | of ducting fall–60 ft of ducting fall per 1,000 | | | | | |
| D3041.103b HVAC fan-capacity: all-equipment | PFA | ft of ducting. Damaged, inoperative but anchorage is OK. | EA 1 | 1 | 3.43 | 5 | 2.81 |
| that is either hard anchored or is vibration | ГГA | Daniaged, moperative but anchorage is OK. | EA I | 1 | 3.43 | 3 | 2.01 |
| isolated with seismic snubbers/restraints-equipment | | | | | | | |
| fragility only | | | | | | | |
| D4011.023a fire sprinkler water piping–horizontal | PFA | Spraying and dripping leakage at joints-0.02 | LM 92.9 | 3 | 0.451 | 10 | 0.369 |
| mains and branches—old style victaulic—thin wall | IIA | leaks per 20 ft section of pipe. | LIVI 92.9 | 5 | 0.431 | 10 | 0.309 |
| steel–poorly designed bracing, SDC D, E, or F, | | Joints break and major leakage–0.02 breaks | | | 0.937 | | 0.313 |
| PIPING FRAGILITY | | per 20 ft section of pipe. | | | 0.751 | | 0.515 |
| D4011.053a fire sprinkler drop standard threaded | PFA | Spraying and dripping leakage at drop | EA 100 | 2 | 0.649 | 5 | 0.531 |
| steel–dropping into braced lay-in tile SOFT | | joints-0.01 leaks per drop. | 2.1100 | - | 0.017 | | 0.001 |
| ceiling-6 ft. long drop maximum, SDC D, E, or F | | Drop joints break and major leakage–0.01 | | | 0.179 | | 0.0612 |
| | | breaks per drop. | | | | | |

Note: EDP = engineering demand parameter; SDR = story drift ratio; Q = quantity; Q = lower quantity; UQ = upper quantity; PFA = peak floor acceleration; LM = linear meter; SM = square meter; TN = ton; and EA = each.

Table 6. REDi repair classes for two-story components

| | Average damage states (\bar{DS}) | | | | |
|--|--------------------------------------|---------------------------|---------------------|--|--|
| Component | $\overline{0 < \overline{DS} \le 1}$ | $1 < \overline{DS} \le 2$ | $\overline{DS} > 2$ | | |
| CLT rocking wall—lateral force-resisting system including PT bars, two CLT walls, and UFP connectors | 3 | 3 | 3 | | |
| Partition walls-gypsum with metal studs-fixed below, slip track above | 1 | 1 | 3 | | |
| Ceiling—suspended ceiling | 1 | 3 | 3 | | |
| Glazing-midrise stick-built curtain wall | 2 | 3 | 3 | | |
| Cooling tower–capacity: <100 t | 2 | _ | _ | | |
| Chiller–capacity: <100 t | 2 | _ | _ | | |
| Compressor-capacity: small non-medical air supply | 2 | _ | _ | | |
| Fire sprinkler drop standard | 2 | 3 | _ | | |
| HVAC fan in line fan | 2 | _ | _ | | |
| HVAC galvanized sheet metal ducting | 3 | 3 | _ | | |
| Fire sprinkler water piping-horizontal mains and branches | 2 | 3 | _ | | |

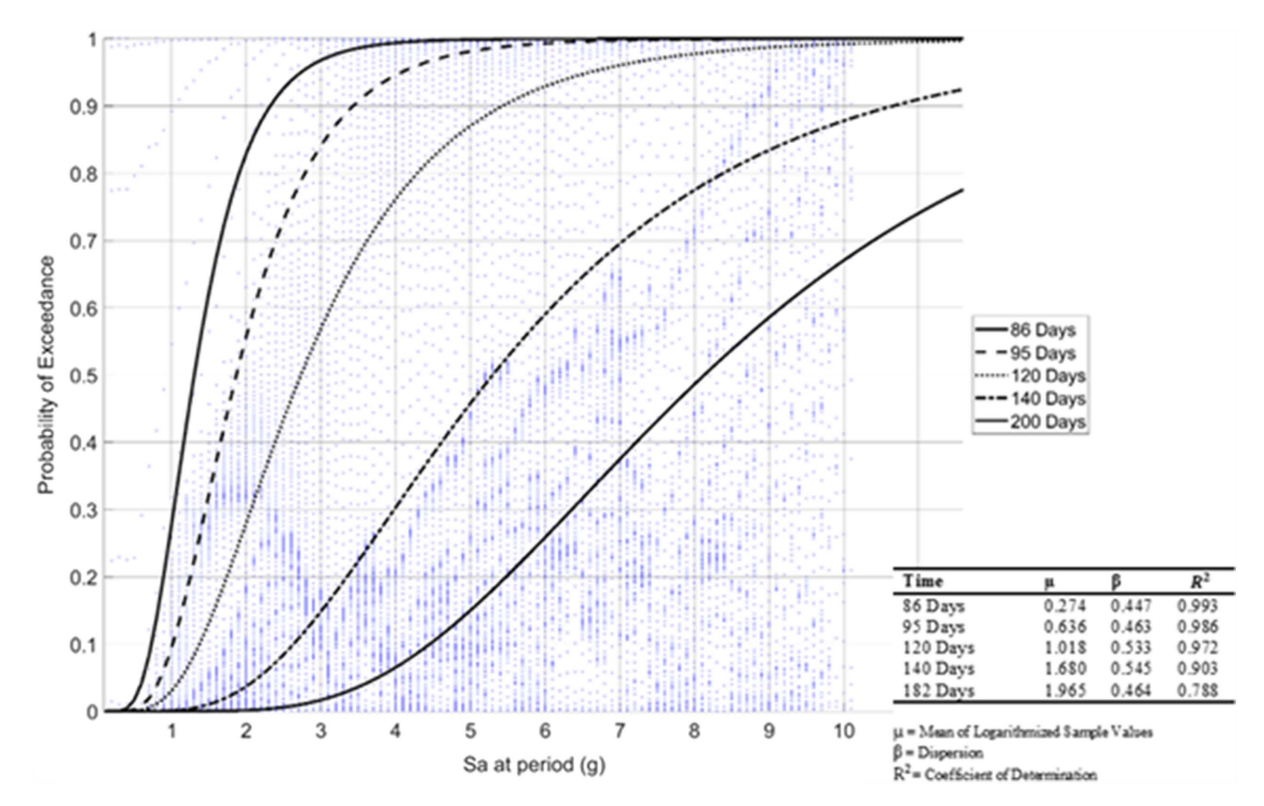


Fig. 7. Reoccupancy TTF fragility curves at the natural period of the two-story building.

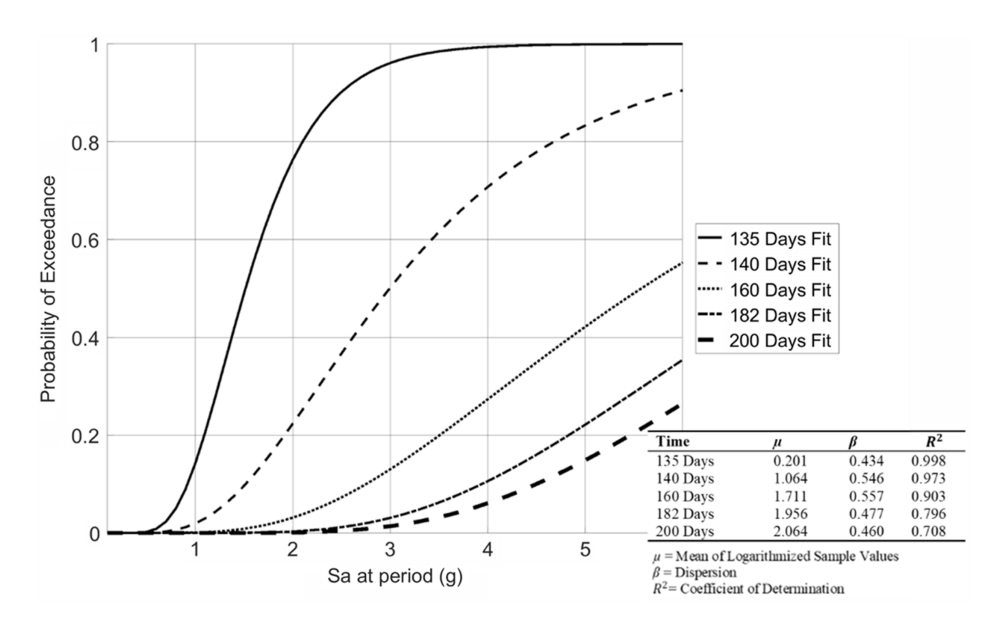


Fig. 8. Functional recovery TTF fragility curves at the natural period of the two-story building.

minor damage to the structure that represents a lower probability of occurrence. There also seems to be a correlation between the increasing number of repair days and a noticeable reduction in the \mathbb{R}^2 value of the lognormal curve fits. This correlation can be attributed to the flattening of the curves as time increases. In other words, the probability of exceedance increases with increasing Sa slower for larger TTF times than in lesser TTF values, which is expected.

The lognormal curve fits in Fig. 7 directly represents the probability that a reoccupancy time (i.e., 86 days and 95 days) is exceeded at a given spectral acceleration. For example, at a spectral

acceleration of 2 g, the two-story CLT structure has approximately a 0.83 (83%) probability of exceeding 86 days for reoccupancy while simultaneously having a 0.26 (26%) chance of exceeding 120 days. This can be further applied to estimate TTF performance for specific events using the approximated event spectral acceleration at the structure's period. Figs. 8 and 9 show the corresponding fragility curves for functional recovery and full recovery, respectively.

The fragility curves for functional recovery and full recovery are observed to be nearly identical; the only visible difference is for the

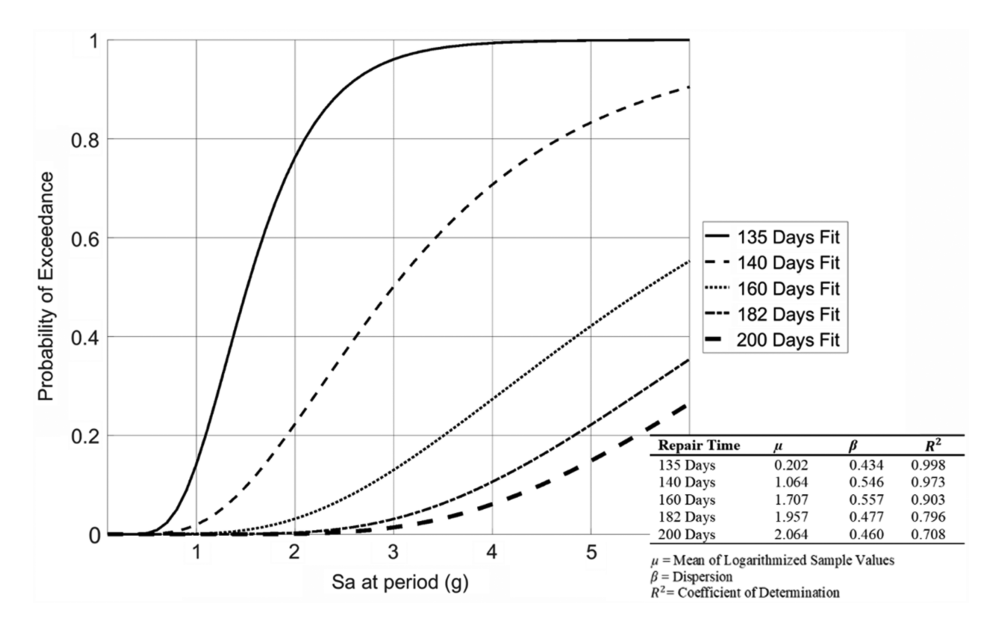


Fig. 9. Full recovery TTF fragility curves at the natural period of the two-story building

135- and 160-day fit data. This result is entirely due to the component selection and its corresponding repair class associations. More specifically, it is unique to the illustrative example herein and will most likely not hold for other buildings and component configurations with increased complexity. No general conclusions about the relationship between functional and full recovery should be drawn from this result. Full recovery is defined as the restoration of the structure to its preevent level, which corresponds to the repair of all components in repair classes 1, 2, and 3; while functional recovery is defined as the minimum amount of repair needed to restore functionality to the structure, which corresponds to the repair of all components in repair classes 2 and 3. Further investigation of the behavior of the model suggests that at larger spectral accelerations (larger damage states), all components are more heavily damaged and thus fall into repair class 2 or 3 (Table 5). This means that by definition, at larger spectral accelerations, full recovery is equal to functional recovery. For moderate spectral accelerations, HVAC components do not have a damage state for repair class 1 and are instead always considered repair class 2 (Table 5). This is important to note because these components have long lead times associated with them, meaning that repair class 1 components can be repaired while waiting for the repair class 2 components to arrive, thus leading to the functional recovery and full recovery being equivalent. Finally, at lower spectral accelerations, the HVAC components will not be damaged, while several components will be in their repair class 1 damage state. This leads to the reoccupancy and functional recovery being equivalent, while the full recovery is larger. Recalling the observed difference between the functional recovery and full recovery of the 135 days and 160 days TTF fragility curves, respectively, and combining this observation with the previously discussed lower sample densities at quicker TTF values, one can conclude that the demonstrated difference between the TTF fragility curves is due to samples at low spectral accelerations affecting the fit for both 135 and 160 days. Functional recovery and full recovery are not expected to be so similar for every structure; incorporation of more resilient components, repair class 1 components with long lead times, different repair class 2 components, and among other things could all differentiate the functional recovery and full recovery significantly.

Conclusions

The methodology laid out in this study allows for the development of TTF fragility curves that incorporate both structural and nonstructural components, as well as a variety of uncertainties. The primary contribution of this study is the methodology that merges a REDi downtime assessment methodology and FEMA P-58 methodology into a multilayered direct Monte Carlo simulation to develop TTF fragility curves in terms of the time required to achieve different levels of system recovery. Families of TTF fragility curves representing those building states can provide, at a glance, a fairly comprehensive and clear view of the probability of a structure over a variety of different demand parameters, lending itself well to its incorporation into a larger decision framework. The methodology was applied to a two-story CLT rocking wall structure, but it is applicable to any building or structure with the corresponding fragility and repair time data available for its components, allowing for the application of the method to other common buildings in the inventory.

The rocking wall system reduces the damage to the structural systems of the building and almost entirely eliminates residual drift, but with the drift criteria similar to other systems, it does little to reduce the drift-induced damage for nonstructural components. While the structural components remain mostly undamaged (for practical considerations), the rocking wall system does not reduce damage for most traditional nonstructural elements, demonstrating a need to incorporate more deformation-compatible nonstructural components to improve the resilience of the system. Additionally, while the system here incorporated dropped suspended ceilings, in many cases mass timber buildings less than 6 stories do not incorporate suspended ceilings, reducing the TTF of the structure. Currently, the model estimates the TTF for different recovery levels, allowing for flexibility in the determination of functionality objectives. Additionally, the repair sequencing used in the example was a relatively unmodified implementation of REDi, and while fairly comprehensive, the methodology is not beholden to this type of repair sequencing. It would be possible to modify or completely replace that procedure with a different downtime estimation procedure such as those existing approaches described earlier as more detailed information becomes available. Comprehensively, the effectiveness and potential of the methodology have been demonstrated by the example herein, but areas in which more research is needed have been revealed. The effects of the selected ground motions, analysis type, and *building performance model* complexity need to be further investigated. A sensitivity analysis is needed on the effect of the sampling method and the number of samples of the various distributions has on TTF fragility curves. This study also revealed a need for the development of additional fragility curves for resilient nonstructural components and mass timber products, particularly, gravity connections as the scenario presented herein with minimal damage occurring to these connections will not always apply.

Data Availability Statement

Some or all data, models, or code generated or used during the study are available from the corresponding author by request.

Acknowledgments

This research project is supported by the National Science Foundation through a number of collaborative awards including: CMMI 1636164, CMMI 1634204, CMMI 1635363, CMMI 1635227, CMMI 1635156, and CMMI 1634628. The use of the NHERI experimental facility is supported by the National Science Foundation's Natural Hazards Engineering Research Infrastructure Program. The authors would also like to acknowledge support for the two-story shake table testing program from industry partners including: Katerra, Simpson Strong-Tie, Forest Products Laboratory, Softwood Lumber Board, DR Johnson Lumber, and the City of Springfield, Oregon. The opinions presented here are solely those of the authors. The authors also would like to acknowledge individual industry collaborators and students who worked on this project including Leonardo Rodrigues, Brian Demeza, Gabriele Tamagnone, Daniel Griesenauer, Ethan Judy, Steven Kordziel, Aleesha Busch, Ali Hansan, Joycelyn Ng, Monica Y. Liu, Ata Mohseni, and Da Huang. Additionally, the authors acknowledge other TallWood PI's, namely, Jim Ricles, and Richard Sause for their expertise and insight.

References

- Akbas, T., et al. 2017. "Analytical and experimental lateral-load response of self-centering posttensioned CLT walls." *J. Struct. Eng.* 143 (6): 04017019. https://doi.org/10.1061/(ASCE)ST.1943-541X.0001733.
- Almufti, I., and M. Willford. 2013. "REDiTM rating system." Accessed May 6, 2019. https://www.arup.com/perspectives/publications/research/section/redi-rating-system.
- Amini, O., J. W. van de Lindt, S. Pei, D. Rammer, P. Line, and M. Popovski. 2014. "Overview of a project to quantify seismic performance factors for cross laminated timber structures in the United States." In Vol. 9 of Materials and joints in timber structures: Recent developments of technology, 531–541. Berlin: Springer. https://doi.org/10.1007/978-94-007-7811-5.
- Baird, A., T. Smith, A. Palermo, and S. Pampanin. 2014. "Experimental and numerical study of U-shaped flexural plated (UFP) dissipators." In Proc., New Zealand Society for Earthquake Engineering 2014 Technical Conf. and AGM 2014. Wellington, New Zealand: New Zealand Society for Earthquake Engineering.
- Baker, J. W. 2015. "Efficient analytical fragility function fitting using dynamic structural analysis." *Earthquake Spectra* 31 (1): 579–599. https://doi.org/10.1193/021113EQS025M.

- Barbosa, A. R., A. Sinba, C. Higgins, and R. Soti. 2018. Structural testing for the Dr. Johnson's CLT panels. Corvallis, OR: Oregon State Univ
- Buchanan, A., B. Deam, M. Fragiacomo, S. Pampanin, and A. Palermo. 2008. "Multi-storey prestressed timber buildings in New Zealand." Struct. Eng. Int. 18 (2): 166–173. https://doi.org/10.2749/10168660878 4218635
- Ceccotti, A., C. Sandhaas, M. Okabe, M. Yasumura, C. Minowa, and N. Kawai. 2013. "SOFIE project—3D shaking table test on a seven-storey full-scale cross-laminated building." *Earthquake Eng. Struct. Dyn.* 42 (13): 2003–2021. https://doi.org/10.1002/eqe.2309.
- Cimellaro, G. P., A. M. Reinhorn, and M. Bruneau. 2010. "Framework for analytical quantification of disaster resilience." *Eng. Struct.* 32 (11): 3639–3649. https://doi.org/10.1016/j.engstruct.2010.08.008.
- Cutfield, M., K. Ryan, and Q. Ma. 2016. "Comparative life cycle analysis of conventional and base-isolated buildings." *Earthquake Spectra* 32 (1): 323–343. https://doi.org/10.1193/032414EQS040M.
- Dujic, B., J. Pucelj, and R. Zarnic. 2004. "Testing of racking behavior of massive wooden wall panels." In Proc., 37th CIB-W18 Meeting, Int. Council for Building Research and Innovation. Karlsruhe, Germany: Univ. of Karlsruhe.
- Dujic, B., and R. Zarnic. 2006. "Study of lateral resistance of massive X-Lam wooden wall system subjected to horizontal loads." In *Proc.*, COST E29 Int. Workshop on Earthquake Engineering on Timber Structures, 97–104. Brussels, Belgium: European Cooperation in Science and Technology.
- Ellingwood, B. R., H. Cutler, P. Gardoni, W. G. Peacock, J. W. van de Lindt, and N. Wang. 2016. "The Centerville virtual community: A fully integrated decision model of interacting physical and social infrastructure systems." J. Sustainable Resilient Infrastruct. 1 (3–4): 95–107. https://doi.org/10.1080/23789689.2016.1255000.
- FEMA. 2009. Quantification of building seismic performance factors. FEMA P695. Washington, DC: FEMA.
- FEMA. 2012a. "The performance assessment calculation tool (PACT)." Accessed March 5, 2019. https://www.atcouncil.org/53projects/85-atc -58-project.
- FEMA. 2012b. Seismic performance assessment of buildings. FEMA P-58-1. Washington, DC: FEMA.
- Ganey, R., J. Berman, T. Akbas, S. Loftus, J. D. Dolan, R. Sause, J. Ricles, S. Pei, J. W. van de Lindt, and H. Blomgren. 2017. "Experimental investigation of self-centering cross-laminated timber walls." *J. Struct. Eng.* 143 (10): 04017135. https://doi.org/10.1061/(ASCE)ST.1943-541X .0001877.
- Ganey, R. S. 2015. "Seismic design and testing of rocking cross laminated timber walls." M.S. thesis, Dept. of Civil and Environmental Engineering, Univ. of Washington.
- Hasani, H., K. Ryan, A. Amer, J. M. Ricles, and R. Sause. 2018. "Pre-test seismic evaluation of drywall partition walls integrated with a timber rocking wall." In *Proc.*, 11th US National Conf. on Earthquake Engineering. Oakland, CA: Earthquake Engineering Research Institute.
- Holden, A., C. Devereux, S. Haydon, A. Buchanan, and S. Pampanin. 2012. "Innovative structural design of a three storey post-tensioned timber building." In *Proc.*, *World Conf. on Timber Engineering (WCTE)*, 323–330. Auckland, New Zealand: WCTE 2012 Committee.
- Mayes, R., N. Wetzel, K. Tam, B. Weaver, A. Brown, and D. Pietra. 2013. "Performance based design of buildings to assess damage and down-time and implement a rating system." *Bull. N. Z. Soc. Earthquake Eng.* 46 (1): 40–55. https://doi.org/10.5459/bnzsee.46.1.40-55.
- Mazzoni, S., F. McKenna, M. Scott, and G. Fenves. 2009. "Pacific earth-quake engineering research center." In *Open systems for earthquake engineering simulation user command-language manual—OpenSees version-2.0.* Berkeley, CA: Univ. of California.
- Mitrani-Reiser, J. 2008. *Risk management products team downtime model*. FEMA P-58/BD-3.7.7. Washington, DC: FEMA.
- Mosqueda, G. 2016. *Interior cold-formed steel framed gypsum partition walls*. FEMA P-58/BD-3.9.32. Washington, DC: FEMA.
- Palermo, A., S. Pampanin, M. Fragiacomo, A. H. Buchanan, and B. L. Deam. 2006. "Innovative seismic solutions for multi-storey LVL timber

- buildings." In *Proc.*, 9th World Conf. on Timber Engineering WCTE 2006, 6–10. Corvallis, OR: Oregon State Univ. Conference Services.
- Pei, S., M. Popovski, and J. W. van de Lindt. 2013. "Analytical study on seismic force modification factors for cross-laminated timber buildings." Can. J. Civ. Eng. 40 (9): 887–896. https://doi.org/10.1139/cjce -2013-0021.
- Pei, S., D. Rammer, M. Popovski, T. Williamson, P. Line, and J. van de Lindt. 2016. "An overview of CLT research and implementation in North America." In *Proc.*, World Conf. on Timber Engineering (WCTE 2016). Vienna, AT: Vienna Univ. of Technology.
- Pei, S., J. W. van de Lindt, A. Barbosa, J. Berman, E. McDonnell, J. D. Dolan, H. Blomgren, R. Zimmerman, D. Huang, and S. Wichman. 2019. "Experimental seismic response of a resilient two-story mass timber building with post-tensioned rocking walls." *J. Struct. Eng.* 145 (11): 04019120. https://doi.org/10.1061/(ASCE)ST.1943-541X .0002382.
- Popovski, M., and I. Gavric. 2016. "Performance of a 2-Story CLT house subjected to lateral loads." J. Struct. Eng. 142 (4): E4015006. https://doi. org/10.1061/(ASCE)ST.1943-541X.0001315.
- Popovski, M., and E. Karacabeyli. 2012. "Seismic behaviour of crosslaminated timber structures." In *Proc.*, World Conf. on Timber Engineering 2012. Auckland, New Zealand: New Zealand Timber Design Society.
- Popovski, M., J. Schneider, and M. Schweinsteiger. 2010. "Lateral load resistance of cross-laminated wood panels." In World Conf. on Timber Engineering, 20–24. Rome: Italian National Research Council.
- Porter, K. 2009a. Fragility of air compressors. FEMA P-58/BD-3.9.20. Washington, DC: FEMA.
- Porter, K. 2009b. Fragility of chillers. FEMA P-58/BD-3.9.15. Washington, DC: FEMA.
- Porter, K. 2009c. Fragility of cooling tower. FEMA P-58/BD-3.9.28. Washington, DC: FEMA.

- Sahabi, A., E. Reis, and D. Khorram. 2018. The case for earthquake resilience: Why safer structures protect and promote social and economic vitality. Washington, DC: US Resiliency Council.
- Spieth, H. A., A. J. Carr, S. Pampanin, A. G. Murahidy, and J. Mander. 2004. Modeling of precast prestressed concrete gram structures with rocking beam-column connections. Christchurch, New Zealand: Univ. of Canterbury.
- Terzic, V., S. Mahin, and M. Comerio.2014. "Comparative life-cycle cost and performance analysis of structural systems for buildings." In *Proc.*, 10th US National Conf. on Earthquake Engineering: Frontiers of Earthquake Engineering. Oakland, CA: Earthquake Engineering Research Institute.
- Terzic, V., S. K. Merrifield, and S. Mahin. 2012. Lifecycle cost comparisons of different structural systems. Berkeley, CA: Structural Engineers Association of California.
- Terzic, V., D. Yoo, and A. H. Aryan. 2016. "Repair time model for buildings considering the earthquake hazard." In *Proc.*, *Implementation Manual USRC Building Rating System for Earthquake Hazards*. Sacramento, CA: Structural Engineers Association of California.
- Vamvatsikos, D., and C. Cornell. 2002. "Incremental dynamic analysis." *Earthquake Eng. Struct. Dyn.* 31 (3): 491–514. https://doi.org/10.1002/ege.141.
- Yamin, L., A. Hurtado, R. Rincon Garcia, J. Dorado, and J. Reyes. 2017. "Probabilistic seismic vulnerability assessment of buildings in terms of economic losses." *Eng. Struct.* 138 (2): 308–323. https://doi.org/10.1016/j.engstruct.2017.02.013.
- Yang, T., J. Moehle, B. Stojadinovic, and A. Kiureghian. 2009. "Seismic performance evaluation of facilities: Methodology and implementation." *J. Struct. Eng.* 135 (10): 1146–1154. https://doi.org/10.1061/(ASCE)0733 -9445(2009)135:10(1146).
- Zeng, X., X. Lu, T. Y. Yang, and Z. Xu. 2016. "Application of the FEMA-P58 methodology for regional earthquake loss prediction." *Nat. Hazards* 83 (1): 177–192. https://doi.org/10.1007/s11069-016-2307-z.